Role of vibration in solid-liquid separation using a vacuum belt filter

P. Broadbridge[1] S. Caldwell[2] T. Marsh[3]
M. McGuinness[4] O. Orozovic[5] D. I. Pontin[6]
A. Raboonik[7] K. Stevens[8]

(Received 29 July 2022; revised 10 January 2023)

Abstract

Modelling and analysis are carried out for stages of de-watering mineral slurry on a vacuum-belt filter, with a patented vibrating roller module called 'Viper' situated atop the formed cake. The long-term goal here is to improve the efficacy of the dewatering since enhancements by as little as 1% solid mass fraction have significant economic benefits. We show that Darcy's law accurately models the dewatering process through a clogging filter mat until no more water can be extracted using mere vacuuming, and the predicted solid mass fraction is in accordance with available data. It is shown that after this initial de-watering stage, air fingers are formed in accordance with Saffman–Taylor theory, thereby releasing the hydraulic pressure gradient and de-watering ceases as a result. The Viper units break up these fingers, thus facilitating

DOI:10.21914/anziamj.v64.17561, Published 2023-02-16, as part of the Proceedings of the 2022 Mathematics and Statistics in Industry Study Group. ISSN 1445-8810. (Print two pages per sheet of paper.)

further de-watering. Estimates of the time span of development of the air fingers are made using extended Saffman–Taylor theory and these are used to determine the optimal spacing of the Viper units. At the vibrational frequencies used in Viper units, the estimated Deborah number is small enough so that liquefaction is expected to occur; this would explain the efficacy of the Viper device.

Contents

1 Introduction

This is a group report on a challenge brought to the February 2022 Mathematics in Industry Study Group hosted by the University of Newcastle in Australia. Jord International (NSW, Australia) asked the Study Group to develop a mathematical model that could help to improve the dewatering of slurry in a vacuum-belt filter when using Viper technology.

During the early stages of processing and refinement, mineral ores are crushed and mixed with water to form a slurry. At some stage, the solids must be separated and the water returned to a pond. Incremental improvements in solid mass fractions by as little as 1% may have large economic benefits.

One method used world-wide is the vacuum belt filter. A conveyor belt, typically 30 m long, conveys the mixture, typically for three minutes. During that time, a vacuum pump system maintains the pressure below the belt at around 0.7 atmospheres. The surface of the slurry above the belt is at a pressure of one atmosphere, P_{atm}.

The resulting pressure gradient drives the liquid downwards through perforations in the belt. Solid particles are collected on a filter mat of around 2.5 mm thickness attached to the belt. In the data on crushed coal slurry provided by the Jord company, the slurry enters at a depth of around 15 cm and at 18% solids by mass (wet basis). The material leaves as a well-formed cohesive cake containing 70% or more solids by mass.

Jord found that the final solid mass content is improved to 75% if the newly formed cake, with negligible overlying water at around 16–18 m along the belt, passes under a 30 cm roller whose axle is attached to a Viper that vibrates at frequency 50 Hz and amplitude 2 mm (Figure 1).

A mathematical model for this operation is sought, in the hope that it will lead to a better understanding of the process. In the future, the model may provide guidance as to how to optimise performance, for example to help decide the optimal number and placement of the Viper units.

Figure 1: Schematic layout of working vacuum belt (not to scale).

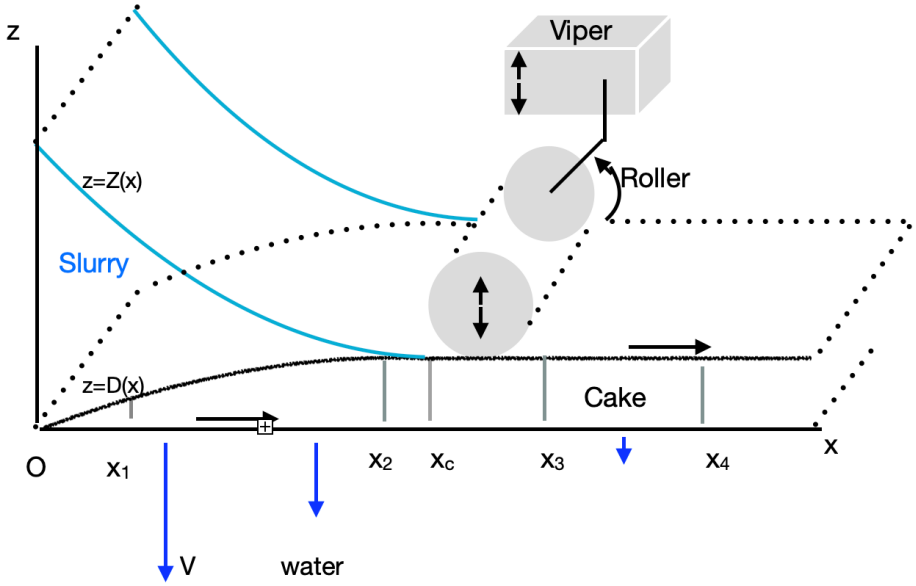

The solid/fluid mixture has different characteristics along three distinct segments of the belt. They are the super-saturated slurry region at the input end, the unsaturated cake at the far end, and the emergent cake which is saturated over a few metres in the intermediate region where a thin film of water is observed above its surface. The Viper often operates in this region, see Figure 1.

Along the belt, water is drawn through a filter mat of thickness 2.5 mm, leaving behind a sediment consisting of solid particles that form a porous matrix.

From the geometry of the system it is convenient to use Cartesian coordinates x for horizontal distance along the belt and z for vertical distance above the belt. In experiments little variation is observed in the third dimension, labelled by horizontal distance y from one edge across the width of the belt, and

variation in this direction is not considered in our modelling. The belt width associated with the collected data is 4.2 m.

In a reference frame attached to the belt, the sediment layer has an increasing height $D(t)$. At x values in the range $0 < x < x_c$, above the sediment there is a liquid slurry up to height $Z(t)$ that is decreasing in time as water is removed. Define $Z_0 = Z(0)$ which is taken to be 15 cm, from the data supplied by Jord for a particular implementation.

In a reference frame attached to the ground, the belt moves at uniform velocity $\dot{x} = u_0$ and the time averaged steady profile is $Z(x/u_0)$ for the slurry surface and $D(x/u_0)$ for the sediment surface.

At a critical location $x = x_c$ there is a form line where $Z - D = 0$ and the uncovered cake surface emerges. The cake is already close to its final height which is observed to be $D_c = 4.0$ cm. The form line has some curvature but that is neglected in our one-dimensional model.

From measured solid mass fractions f_s sampled at stations $x = 15$ m and 18 m it is known that x_c is intermediate between those two values. At $x = 16.5$ m , the roller interacts with saturated pliable formed cake. In the example calculations the form line is predicted a priori to be at $x_c = 16.0$ m .

For a short distance thereafter, there are some fluctuations of depth of an overlying thin film as surface water waves ebb and flow. This is the region where the roller and Viper are often placed. At larger values of x, the cake is unsaturated as progressively more water is removed, leaving air-filled channels.

2 The Super-Saturated Slurry

In the industry, concentrations are most conveniently expressed in terms of the solid mass fraction f_s. For flow through porous media, the state of the system is conventionally expressed in terms of volumetric water concentration θ. It is useful to convert between these two descriptions. Consider a sample of

mass M and volume $\mathcal{V}$ separated into solid and liquid water components. Densities of the solid and liquid components are ρ_s and ρ_w. At the slurry boundary locations $x = 0$ and $x = x_c$ there is one free boundary. The mixture is close to uniform, with one solid and one fluid component. In that situation, for a local sample of mass M and volume $\mathcal{V}$,

$$M = \rho_w \theta \mathcal{V} + \rho_s (1-\theta)\mathcal{V}, \qquad f_s = \frac{\rho_s \mathcal{V}(1-\theta)}{\rho_s \mathcal{V}(1-\theta) + \rho_w \mathcal{V}\theta},$$
$$\iff \theta = \frac{(1-f_s)(\rho_s/\rho_w)}{1 + (1-f_s)(\rho_s/\rho_w - 1)}.$$

For anthracite, the relative density is typically $\rho_s/\rho_w = 1.4$. At the inlet $f_s = 0.18$ so volumetric water content is $\theta_0 = 0.865$. This exceeds the porosity of any known sediment, with soil porosities being less than 0.6. This means that the mixture is a slurry within which the solid particles are not connected, offering little resistance to water flow.

Below the belt, the vacuum system lowers the pressure to 0.7 atmospheres, $P = 0.7 P_{\text{atm}}$. Therefore the flow is predominantly downwards. Hence it is reasonable to consider a quasi-one-dimensional flow.

In a reference frame attached to the belt, the mass and volume of solid within a vertical slice is constant. Therefore at the form-line location x_c where the mixture has depth D_c and water content θ_c, the equivalent depth of pure solid is $D_s = 2.00\,\text{cm}$. Then

$$D_c(1-\theta_c) = Z_0(1-\theta_0) = 2.00\,\text{cm} \quad \text{(constant)}.$$

Assuming $D_c = 4.00\,\text{cm}$, this equation gives $\theta_c = 0.500$. Since at this location the porous matrix is fully saturated with no slurry visible on top, θ_c is the saturated water content, conventionally labelled as θ_s. This provides an estimate of the porosity. By comparison, the standard Yolo light clay has the practically identical value $\theta_s = 0.495$ (e.g., Smith et al. 2002). A fitted Darcy flow model, developed below, predicts $D_c = 3.65\,\text{cm}$ and $\theta_c = 0.451$.

In the region $0 < x < x_c$, $D > 0$ and $Z - D > 0$, since gravity forces are weak compared to the pressure gradient of the vacuum system, we assume that gravitational settling is negligible. Then $\theta = \theta_0$ for $D < z < Z$ and $\theta = \theta_c$ for $0 < z < D$. The thin boundary layer that connects these two values is ignored. Assuming that the solid volume in a vertical slice remains constant, the mass partitioning generalises to

$$[Z - D][1 - \theta_0] + D(1 - \theta_c) = D_s \text{ (constant)}. \tag{1}$$

2.1 Darcy Flow Model

The total hydraulic head (e.g., Smith et al. 2002) is $H = h + z - Z_0$ where

$$h = \frac{P - P_{atm}}{\rho_w g}.$$

The pressure head h is conventionally set to be zero at atmospheric pressure which occurs at $z = Z$. The other term $z - Z_0$ is due to the gravity force. At static equilibrium in one dimension, $H = h + z - Z_0 = 0$ (constant) so that the gradient of pressure provides a balance against gravity, $\partial P/\partial z + \rho_w g = 0$.

In the current situation, the liquid is not static but flows downwards. However, since the porous mat and sediment pile provide most of the hydraulic resistance, most of the variation of pressure head occurs across the porous material of total thickness $D + D_m$ where $D_m = 2.5\,\text{mm}$, the thickness of the mat.

During sedimentation, fines clog the larger pores so that saturated hydraulic conductivity K_s decreases with time, or equivalently it decreases with distance x along the belt. Then the vertical Darcy flux

$$V = -K_s(t)\left[\frac{\partial h}{\partial z} + 1\right] = -K_s(t)\left[\frac{c_1}{D(t) + D_m} + 1\right], \tag{2}$$

where

$$c_1 = \frac{0.3 P_{atm}}{\rho_w g} = 3.0\ \text{m}.$$

At the entry point, the depth of slurry adds an additional $0.15\,\mathrm{m}$ to the pressure head. This equates to an additional 5% to the pressure gradient, a contribution that rapidly diminishes as liquid is removed. The Darcy velocity V is the volume of water transported through unit cross section of area in unit time so it has the dimensions of velocity. The actual fluid velocity is V/θ. The fractional contribution of the gravity term to the square bracket in (2) is less than 10^{-3} at the inlet and is $1/70$ at $x = x_c$. Therefore it is neglected in most calculations.

In practice K_s may vary by several orders of magnitude whereas porosity sits between 0.42 and 0.52 for known soils, except for heavy clays that may have porosity as large as 0.6, the additional 0.1 usually being occupied by trapped water. Therefore, in comparison with highly variable K_s, porosity θ_c is approximated as a constant.

As the slurry flows downwards, solids at volumetric concentration $1-\theta_0$ are advected and then deposited at the surface $z = D(t)$. At location x, consider a vertical thin slice of width δx, height Z, base area $\delta A = Y\delta x$ and volume $v = Z\delta A$. There are liquid water and solid mineral components, $v = v_w + v_s$. Now

$$v_w = \theta_0(Z-D)\delta A + \theta_c D\delta A\,,$$
$$v_s = (1-\theta_0)(Z-D)\delta A + (1-\theta_c)D\delta A\,.$$

Solids are retained but water departs through the lower boundary at volumetric flux density V. Hence

$$V\delta A = \dot{v}_w = \theta_0(\dot{Z}-\dot{D})\delta A + \theta_c\dot{D}\delta A\,, \tag{3}$$
$$0 = \dot{v}_s = (1-\theta_0)(\dot{Z}-\dot{D})\delta A + (1-\theta_c)\dot{D}\delta A\,. \tag{4}$$

Substituting (4) into (2) and (3) there follows the differential equation for $D(t)$,

$$\dot{D} = K_s(t)\frac{c_1(\theta_0-\theta_c)}{(1-\theta_0)(D+D_m)}\,,$$

subject to $D = 0$ at $t = 0$. The solution is

$$D(t) = \left[2c_1 \frac{\theta_0 - \theta_c}{1 - \theta_0} \int_0^t K_s(\bar{t})d\bar{t} + D_m^2\right]^{1/2} - D_m\,. \tag{5}$$

Thereafter, $Z(t)$ follows from (1).

It was found that the data for the solid mass fraction $f_s(t)$ could not be reconciled with a constant value K_s or for separate constant values of conductivity for the sediment and the mat in series. However, good agreement was obtained by assuming the form

$$K_s = \frac{K_m}{1 + qt} \quad (q \text{ constant}).$$

The solution does not apply beyond the cake formation time $t = x_c/u_0$ so for current purposes it is not necessary to add a limiting platform value to $K_s(t)$. For that particular model,

$$D(t) = \left[\frac{2c_1 K_m}{q} \frac{\theta_0 - \theta_c}{1 - \theta_0} \log(1 + qt) + D_m^2\right]^{1/2} - D_m\,.$$

Thereafter, $Z(t)$ may be inferred from (1) and subsequently $\theta(t)$ and $f_s(t)$ follow from

$$\theta = \frac{Z - D_s}{Z}\,, \qquad f_s = \frac{D_s \rho_s/\rho_w}{\theta Z + D_s \rho_s/\rho_w}\,. \tag{6}$$

The solution has two unknown parameters K_m and q. These are determined from the two experimental points in the slurry zone, with x given in metres, $(x, f_s) = (3, 0.45)$ and $(x, f_s) = (15, 0.62)$. The results are $q = 3.45\,s^{-1}$ and $K_m = 4.71 \times 10^{-5}$m/s $= 17.00$ cm/h.

It then follows from solving $Z - D = 0$ that $x_c = 16.00$ m and $K(t_c) = K_c = 1.13 \times 10^{-7}$ m/s. The filter mat conductivity K_m sits in the range for a silty sand, whereas the hydraulic conductivity of the formed cake is close to that

Figure 2: Sediment depth D (blue) and slurry depth Z (orange) versus x—solution to model, circle symbols from experimental solid mass fraction.

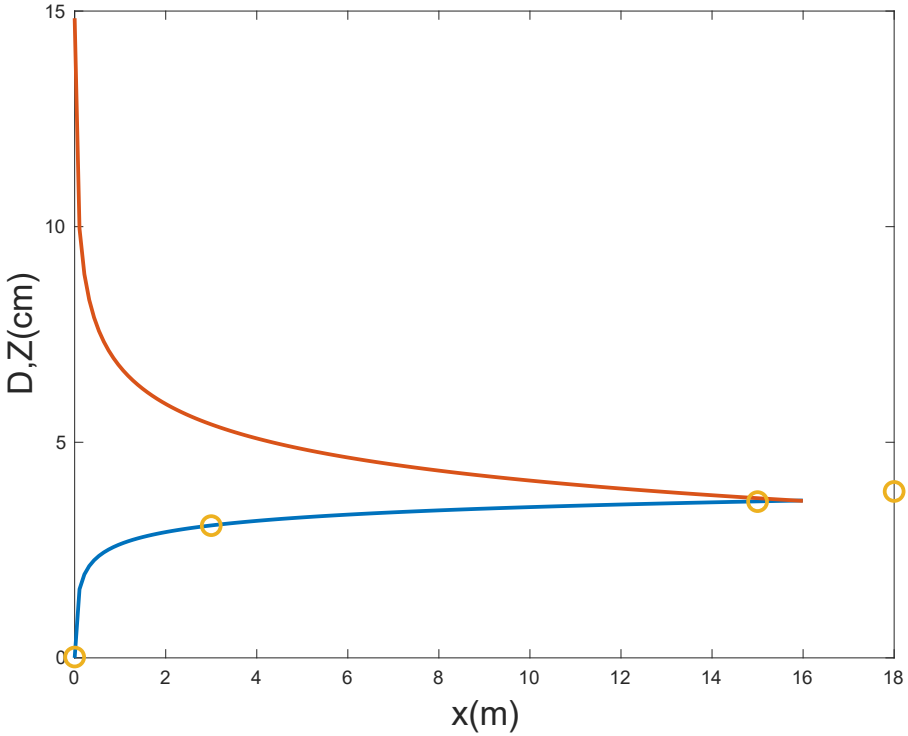

of Yolo light clay (e.g., White and Broadbridge 1988). These values seem reasonable from the mixture of particles in the slurry and cake and the fibres in the mat. The substantial and rapid decrease in K_s over a time of the order of 0.3 s again indicates that a model with constant K_s cannot agree well with the data. K_s may be primarily a function $\mathcal{K}(D)$ of sediment depth D, independent of belt speed u_0. That rapidly decreasing function is

$$\mathcal{K}(D) = K_m \exp\left[\frac{-\rho_w g q}{2K_m \Delta P}\left(\frac{1-\theta_0}{\theta_0-\theta_c}\right) D\left(D+2D_m\right)\right]. \qquad (7)$$

Figures 2 to 4 plot D, Z, θ, and f_s against x.

Figure 3: Volumetric water content θ versus x—solution to model, circle symbols from experimental solid mass fraction.

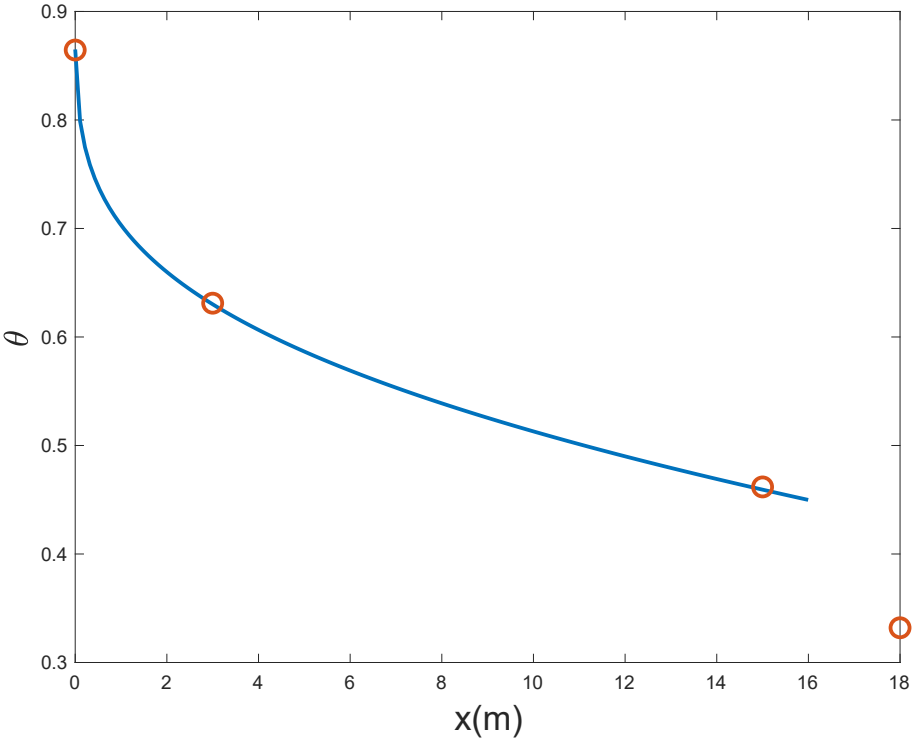

Towards the end of the slurry zone at $x = 15\,\mathrm{m}$, it is found experimentally that $f_s = 0.62$ whether or not the Viper is installed. Then from (1) and (5) at $x = 15\,\mathrm{m}$, the current model has $D = 3.62\,\mathrm{cm}$ and $Z = 3.72\,\mathrm{cm}$. The newly formed cake is predicted to have depth $D_c = 3.65\,\mathrm{cm}$. Experimentally it is observed to be $4\,\mathrm{cm}$. The small under-estimate by the model could be due to the neglect of the horizontal component of flow of solid material in the x direction, which would occur to some extent due to the slope of the free surface of the slurry. The solid mass fraction at the form line f_s agrees exactly with the experimental value 0.63.

Figure 4: Solid mass fraction f_s versus x. Solid curve is solution to model, circle symbols show experimental data.

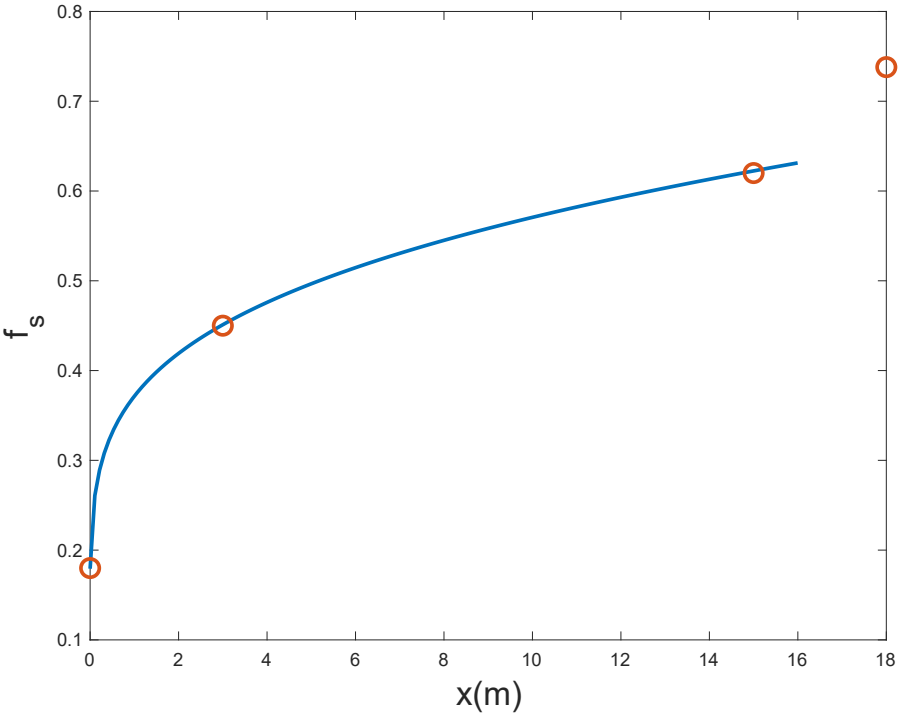

At the inlet, the equivalent depth of water is $\theta_0 D_0 = 13.0\,\text{cm}$. At the form line $x = x_c$, the equivalent depth of pure water is $D_c\theta_c = 1.65\,\text{cm}$. That means that by the form line, 87% of the initial water volume has already been removed from the mixture.

3 The Unsaturated Formed Cake

Beyond the form line, there is no longer water overlying the cake. If more water is forced out of the cake, it is displaced not by water but by air, initially through the larger pores where the surface tension forces that hold the water are weaker. That means that the cake must be unsaturated, with $\theta < \theta_c$. In that unsaturated state, formally h is negative but in the formulations of Buckingham and Richardson independently in the early 20th C (Raats and Knight 2018), $h < 0$ makes sense as the negative potential energy per unit weight of water. Water continues to be pushed through progressively smaller capillaries.

From the experimental data it is found that without the Viper, at the end of the 30 m belt the cake has $f_s = 0.705$ which corresponds to $\theta = 0.321$. At the end of the line, 91% of the initial water volume has been removed, no more than 1% above that which was removed before 18 m.

There are three reasons why water extraction is much less effective through the formed cake. Firstly, after consolidation, the cake has some rigidity and the water cannot easily be squeezed out by further compaction.

Secondly, the air displaces water from the larger pores. Water is now contained in an unsaturated porous medium, held in finer pores so that the hydraulic conductivity is much lower. By comparison, Yolo light clay, which has saturated water content $\theta_s = 0.495$, comparable to that of the coal cake, has its hydraulic conductivity reduced to $0.1K_s$ at $\theta = 0.32$ (e.g., White and Broadbridge 1988). A similar reduction occurs in the unsaturated cake.

Thirdly, the dynamic viscosity ratio μ_a/μ_w between air and water is about 0.02, so we expect the Saffman–Taylor instability to occur with consequent formation of air fingers that are larger than the largest pores. Some of the energy of the vacuum extraction system is wasted as work done in preferentially pushing air at lower resistance, rather than water, through the medium. Another way of looking at this is that the water between fingers is no longer driven out by

the air in the fingers. This further lowers efficiency.

The Saffman–Taylor (Saffman and Taylor 1958) instability shows that a one-dimensional flow solution is not stable but at least in the early wetter stages of the cake, the system favours a two-dimensional solution with a water-air interface that is punctuated by air fingers that reduce water flow. Therefore a solution of quasi one-dimensional flow through the unsaturated cake provides only an upper bound for the amount of water transported.

Compared to the gradient of pressure head $\partial h/\partial z$ in (2), the gravitational component is negligible. Then neglecting gravity, the equation of continuity for quasi one-dimensional flow is $\partial\theta/\partial t + \partial V/\partial z = 0$ which leads to the nonlinear diffusion equation

$$\frac{\partial\theta}{\partial t} = \frac{\partial}{\partial z}\left[\mathcal{D}_w(\theta)\frac{\partial\theta(z,t)}{\partial z}\right], \tag{8}$$

where the water diffusivity

$$\mathcal{D}_w(\theta) = K(\theta)\frac{dh(\theta)}{d\theta}.$$

At low water content, water is held in the finest pores that are resistant to flow. Throughout the unsaturated medium, water diffusivity generally increases with volumetric water content which varies with z.

After the pond depth reduces to zero, it may be assumed that the water flux supplied at the surface is zero. Evaporation rates are negligible, rarely as high as 0.04 cm per hour (1 cm per day) whereas the mean exiting downward water flux over the last 12 m of belt is measured to be at least 3 cm per hour (0.5 mm per minute). At the top boundary we impose a zero-flux boundary condition. At the bottom boundary, the exiting free water at pressure $0.7P_{atm}$ is at equilibrium with pore water at the corresponding value of capillary pressure head $h(\theta) = -0.3P_{atm}/\rho_w g$. That gives a boundary condition $\theta = \theta_0$ at $z = 0$ such that $h(\theta_0) = -0.3P_{atm}/\rho_w g$. Therefore the representative one-dimensional initial boundary value problem is the PDE (8)

subject to initial condition $\theta(z,0)=\theta_c$ with boundary conditions $\theta(z,0)=\theta_c$ and $\theta(0,t)=\theta_0$. The two-parameter representation $D_w=a(b-\theta)^{-2}$ is an integrable model that is suitable for many purposes. A similar problem has been solved exactly on a finite one-dimensional domain with prescribed flux boundary conditions (Broadbridge and Banks 1992). The current problem with mixed boundary conditions would be more difficult.

With the 50 Hz Viper operating, from $x=18\,\mathrm{m}$ which is soon after reconsolidation, 1.00 cm depth of water remains inside the cake but along the remainder of the belt, the additional depth of water removed is only 0.07 cm. At the efflux boundary $z=0$ there is no major end effect due to the limited 4 cm thickness of the cake and the limited 1.0 cm depth of internal water remaining. Therefore according to the theory of nonlinear diffusion, the change in internal water depth over this elapsed time is given approximately by a negative infiltration $I=-S(t-t_3)^{0.5}$ where $t_3=x_3/u_0=135\,\mathrm{s}$ and $I=-7\times10^{-4}\,\mathrm{m}$. That gives an estimate for the desorptivity $S\approx7\times10^{-5}\,\mathrm{m\,s^{-1/2}}$. This is comparable to the sorptivity $1.2\times10^{-4}\,\mathrm{m\,s^{-1/2}}$ of Yolo light clay over a similar range of water contents (White and Broadbridge 1988) when the boundary value and initial value for this problem are interchanged. Not only the saturated hydraulic conductivity but also the sorptivity (closely related to the square root of mean diffusivity) are close to those of a light clay.

3.1 Saffman–Taylor Instability

The Saffman–Taylor instability (Saffman and Taylor 1958; Chuoke, van Meurs, and van der Poel 1959) occurs when a fluid is pumped into a porous medium and displaces a more viscous fluid that is already present. When the cake first appears at the form line on the conveyor, the air at the top of the cake begins to enter and drive the liquid that is inside, down through the cake. Since water is fifty times more viscous than air, at room temperature, conditions are perfect for fingering to occur, after the form line. Prior to the form line, air is not driving water from inside the cake; air pushes down on liquid water

(slurry, really) above the porous medium there, so that within the porous medium there is only one fluid present (with solid grains in it) and viscous fingering is not expected to occur.

The consequence of fingering for getting water out of the cake is severe. Air forms short-cut fingers that eventually reach from the top to the bottom of the cake, leaving behind most of the water. The higher the pressure gradient, the worse the instability, and fingers form more rapidly.

There is no requirement for variations in porosity for this to occur. The instability causing fingers of air to form and penetrate the liquid in the cake is a result of the kinematic boundary condition at the air/liquid interface and of the difference in viscosities of air and liquid water. The surface tension plays a very important role in determining the size of fingers and the speed with which they propagate to the bottom of the cake.

The Viper might well act to disrupt the air fingers that are predicted by Saffman and Taylor's results to be forming in the cake, once liquid is no longer visible at the top, by breaking the fingers and mixing liquid into any fingers of air that have formed.

We now compute the timescale for the growth rate, and wavelength, of the most unstable mode, which requires that we include surface tension. The timescale gives (with belt speed) a distance over which a finger fully develops.

3.1.1 Instability Calculations

Saffman and Taylor (1958) start with Darcy's law for fluids flowing in a porous medium,

$$V = -\frac{k}{\mu}\nabla(p + \rho g z) = \nabla\phi,$$

where z is elevation or height, p is fluid pressure, V is the Darcy velocity of the fluid, $k = K\mu/(\rho g)$ is permeability, K is hydraulic conductivity, ρ is fluid density, $\phi = -K_s H$ is a velocity potential, and μ is the dynamic viscosity.

They consider two superposed incompressible fluids forced by gravity and an imposed vertical pressure gradient across a porous medium, with a steady state of uniform motion with velocity V, and an interface that is horizontal in a rectangular coordinate system (x, y, z). Conventionally, V is taken to be positive when flow is upwards opposing gravity. They perturb the interface that is initially and instantaneously at $z = 0$, deforming it into a corrugation of wavelength $\ell = 2\pi/n$ (where n is wave number) and amplitude a described by

$$z = ae^{iny+\sigma t}.$$

Conservation of mass gives the continuity equation

$$\nabla \cdot V = \nabla^2 \phi = 0\,.$$

Solutions that vanish at infinity and satisfy at $z = 0$ the continuity of normal velocity condition (at leading order in the perturbation)

$$\frac{\partial \phi_1}{\partial z} = \frac{\partial \phi_2}{\partial z} = V + a\sigma e^{iny+\sigma t},$$

take the form

$$\phi_1 = Vz - \left(\frac{a\sigma}{n}\right) e^{iny-nz+\sigma t}, \qquad \phi_2 = Vz + \left(\frac{a\sigma}{n}\right) e^{iny+nz+\sigma t},$$

where the subscript 1 refers to the upper fluid, and subscript 2 refers to the lower fluid. Then the pressures are

$$p_1 = -\frac{\mu_1}{k_1}\phi_1 - \rho_1 g z\,, \qquad p_2 = -\frac{\mu_2}{k_2}\phi_2 - \rho_2 g z\,, \tag{9}$$

and requiring $p_1 = p_2$ at the interface gives to leading order in a the following relationship between the time growth rate σ and the wavenumber n:

$$\frac{\sigma}{n}\left(\frac{\mu_1}{k_1} + \frac{\mu_2}{k_2}\right) = (\rho_1 - \rho_2)g + \left(\frac{\mu_1}{k_1} - \frac{\mu_2}{k_2}\right) V\,. \tag{10}$$

Instability corresponds to positive (real) σ, when the right-hand side of the above equation is positive. For our case, with air in region 1 overlying water in

region 2, V is negative since flow is downwards, the term in front of V is also negative because air is much less viscous than liquid water (and permeability to air k_1 is bigger than permeability to liquid water k_2, further exacerbating the difference), and the gravity term is negative because liquid water is much denser than air. So gravity is stabilising (giving negative σ values on its own) while the viscosity difference is destabilising (inside the cake) when air pushes downwards on the liquid water. Instability (negative σ) follows whenever

$$|V| > \frac{(\rho_2 - \rho_1)g}{\mu_2/k_2 - \mu_1/k_1}\,. \tag{11}$$

Air permeability k_1 is in general different to liquid permeability k_2, due to gas slippage (the Klinkenberg effect) at the molecular level. They may be close in value, or k_1 may be a factor of ten higher than k_2 (Mahesar et al. 2017).

Viscosities at room temperature are $\mu_1 \approx 1.8 \times 10^{-2}\,\mathrm{mPa\,s}$ and $\mu_2 \approx 1\,\mathrm{mPa\,s}$. So the air ratio μ_1/k_1 is several orders of magnitude smaller than μ_2/k_2, and the differences and the sums of μ_1/k_1 and μ_2/k_2 are well-approximated by μ_2/k_2.

Hence using $K = k\rho g/\mu$ the right-hand side of (11) is approximated by

$$\frac{(\rho_2 - \rho_1)g}{\mu_2/k_2 - \mu_1/k_1} \approx \frac{\rho_2 g}{\mu_2/k_2} = K\,,$$

so that (11) is approximately

$$|V| > K\,. \tag{12}$$

Using the hydraulic conductivity at the form line estimated after (6) as $K \approx K_c \approx 10^{-7}\mathrm{m/s}$, from (2) we estimate

$$V \approx -K\left(\frac{c_1}{D + D_m}\right) \approx -10^{-7}\left(\frac{3}{(40 + 2.5)10^{-3}}\right) \approx -10^{-5}\,\mathrm{m/s}\,.$$

Then (12) is satisfied, since $|V| \approx 10^{-5}$ is two orders of magnitude greater than $K \approx 10^{-7}$. The Saffman–Taylor instability is expected to occur once the cake form line appears.

We seek estimates of the most unstable wavelength and its initial growth-rate, providing estimates of how rapidly fingers of air grow after the form line, and of the widths of the fingers. Since the previous analysis gives instability for all wavelengths, we now allow for the effects of surface tension or capillarity at the air/water interface, which are known (Saffman and Taylor 1958; Chuoke, van Meurs, and van der Poel 1959) to provide a wavelength associated with the most rapid growth rate.

We follow Chuoke, van Meurs, and van der Poel (1959) who deal with capillarity a little differently to Saffman and Taylor (1958). Capillary pressure can be written

$$P_c = \gamma \left(\frac{1}{\sqrt{3k}} + \frac{d^2 z}{dy^2} \right) = \gamma \left(\frac{1}{\sqrt{3k}} - a n^2 z \right), \tag{13}$$

where the surface tension is $\gamma \approx 0.064\,\mathrm{N/m}$. The first term on the right-hand side of (13) is the usual one associated with fluid/fluid interfaces at the pore level underlying the macroscopic interface at z, and the second term is due to the curvature of the interface. Then the pressure match at the interface between fluid 1 and fluid 2 becomes $p_1 = p_2 + P_c$, and noting that there are in general also be constants of integration P_1 and P_2 in the expressions (9) for p_1 and p_2, it follows that at zero order in a

$$P_1 = P_2 + \frac{\gamma}{\sqrt{3k}}.$$

Equating the coefficients of a gives the following modification to (10):

$$\frac{\sigma}{n} \left(\frac{\mu_1}{k_1} + \frac{\mu_2}{k_2} \right) = (\rho_1 - \rho_2) g + \left(\frac{\mu_1}{k_1} - \frac{\mu_2}{k_2} \right) V - \gamma n^2.$$

The nice thing about introducing surface tension γ is that we now have a local maximum for the growth rate σ as a function of wave number n, giving a most unstable wave and its growth rate.

We approximate this here by taking advantage of the relatively small size of our μ_1/k_1 and of the gravity term, to obtain

$$\frac{\sigma}{n}\frac{\mu_2}{k_2} \approx -\frac{\mu_2}{k_2}V - \gamma n^2 = \frac{\mu_2}{k_2}|V| - \gamma n^2. \tag{14}$$

The critical wavelength (all wavelengths above this are unstable) is where the right-hand side of (14) is zero, that is, $\ell_c = 2\pi\sqrt{k_2\gamma/(\mu_2|V|)}$. Setting the derivative of σ with respect to n to zero using (14) gives the most unstable wavelength as

$$\ell_m = \sqrt{3}\ell_c\,.$$

For our parameter values, this is about 1 mm. The value used here for the interfacial surface tension is not really correct in general for a porous medium, as it should be an effective surface tension (Chuoke, van Meurs, and van der Poel 1959). It is only correct for the analogous Hele–Shaw cell model. The effective surface tension is some unknown multiple of γ, so that the actual most unstable wavelengths may be several times larger than 1 mm.

The wavelength value 1 mm gives the growth rate value $\sigma_m \approx 4\,s^{-1}$, so that fingering develops on a relatively rapid timescale of about 1/4 second once the cake makes its appearance. For example, if grain sizes ranging from 50–300 microns are assumed to set the initial perturbation size a at these values, then the perturbation size is ae^{4t} which reaches the full thickness of cake ≈ 40 mm after only a second or two. In this time, the conveyor belt has travelled between 140 and 300 mm, which is of the order of a roller diameter.

Air fingers could break through in a 40 mm cake just 140–300 mm downstream from the form line. This suggests that the first Viper should be placed in that locality.

4 Viper Location and Function

There is scant established scientific knowledge on the behaviour of multiphase fluids in deformable porous media under vibration. Therefore the influence of fingering and liquefaction must be somewhat speculative, to be resolved only by further experimentation. Under the first Viper, we assume fingers of air are disrupted, and we could consider that there is a random mixture of air bubbles and water throughout the cake upon disruption. An approximate result from Saffman–Taylor theory suggests there may be 50% air in the cake by volume upon breakthrough of air fingers. Water and air bubbles do not mix well; it would be a rough approximation to model the mixture after breakup by the Viper, as an equivalent fluid with an effective viscosity that is between air and liquid water values, perhaps halfway between. Then the next occurrence of the viscous instability would not develop as rapidly as before the first Viper, since the viscosity difference is now halved. The maximum time constant σ is approximately proportional to the square root of effective liquid viscosity, so the distance from the Viper to the next breakthrough of the roughed-up cake could be expected to be about a factor of $\sqrt{2} \approx 1.4$ times the first distance, that is, about an extra half again of 140–300 mm. This suggests placing a second Viper at a distance of 200–450 mm from the first Viper.

A third Viper might be placed a further factor of $\sqrt{2}$ away from the second Viper, that is, 300–700 mm away. These estimates of best placement of Vipers being further and further apart assume a similar process of halving the effective viscosity difference between air and mixture each time penetrating fingers are mixed up by a Viper.

With a single Viper operating at 50 Hz, the final solid mass fraction f_s increases from 0.705 to 0.75. This is equivalent to the final water content θ decreasing from 0.321 to 0.256. Then 93% of initial water volume is removed, compared to 91% without the Viper. This change has significant economic consequences as well as improvement in safe stable transport. Every part of the cake surface interacts with the roller of diameter 30 cm, at some time.

The roller has a contact length of around 5 cm with the surface of the pliable cake. The contact time is around 0.36 s. At oscillation frequency $\nu = 50$ Hz, around 18 cycles of vibration take place in that time.

Jord International provided mass fractions obtained from samples at measurement stations at various locations along the belt. The data set is not for publication but some particular measurements are used to inform the modelling team. In the slurry at Station 2 location $x = 15$ m, at a short distance upstream from the form line and the roller, samples have solid mass fraction $f_s = 0.62$ whether or not the viper is operating. However, at Station 3 location $x = 18$ m, just beyond the usual location of the Viper, its operation improves the solid mass fraction from 68.7% to 73.8%. In the 8.5 m from Station 4 to Station 5, very little additional water is removed. With the Viper operating, over the final 8.5 m an additional equivalent depth 0.3 mm of water is removed. Without the Viper, a slightly larger amount, an equivalent depth of 0.8 mm, is removed over that distance. This is because the water content is still higher and the hydraulic conductivity is higher than if the Viper had operated to remove water earlier. The Viper operation still achieves more water extraction over the whole belt passage, mainly near the form line. Clearly the Viper is having a local effect on the passing cake but no local effect on the preceding slurry.

4.1 Squeezing the Sponge

As it reaches Station 3 after passing the Viper, the cake has equivalent water depth reduced 2.5 mm further than when the Viper is not present. This compares with the amplitude of oscillation of the roller axis, $a = 2$ mm. If the roller at its highest elevation is still touching the cake, then it is 4 mm deeper after one half cycle. All solids are retained in the cake so this 2 mm reduction can be compensated only by shrinkage of the cake or by displacement of water by air. While the cake is being rolled, air cannot be entering through the roller. Imagine a saturated sponge being drawn under a roller where it is compressed.

Some water exits at the lower boundary if it is perforated. Some water exits on the upper boundary on the upstream side. In the case of the conveyor belt, the additional water (less than 2 mm in depth) mixes with the slurry from where it is more easily extracted by the vacuum system. However, this cannot be the whole story since, as yet, there is no explanation of the observed frequency dependence. The data show clearly that water extraction is more efficient at 50 Hz Viper frequency than at 15 Hz. At Station 3, f_s reduces from 0.738 to 0.707 when frequency is reduced from 50 Hz to 15 Hz. The equivalent depth of pore water increases from 1.0 cm to 1.16 cm.

4.2 Conditions for liquefaction

Liquefaction can cause saturated soils to flow, for example in earthquakes. The principal mechanism is thought to be the "pressurisation" of the fluid in the pores, which when sufficiently large can overcome the inter-grain forces. The exact mechanism by which the pressurisation occurs is not fully understood and may be different in different applications (e.g., Sawicki and Mierczyński 2006; Goren et al. 2011; Lakeland, Rechenmacher, and Ghanem 2014). In the traditional approach for earthquake modelling it is assumed that there is no drainage from the soil (upwards or downwards) on the timescale of liquefaction, but this has been disputed more recently.

During the operation of the Viper, liquid is seen pooling on the top surface downstream, even when the Viper is positioned where the cake is fully formed. This suggests that the roller/Viper assembly leads to a pressure increase, with the fluid being forced upwards, meaning that drainage is taking place.

To determine whether liquefaction could be at play we need a quantitative analysis. We first follow the calculations of Lakeland, Rechenmacher, and Ghanem (2014). They derive a 1D fluid equation in the vertical direction, coupling Darcy's law with conservation of mass and energy, formulated for a thin vertical slice. Following appropriate expansions and non-dimensionalisations they arrive at the following equation for the variation of the non-dimensional

pressure perturbation P' with time, t:

$$\frac{\partial P'}{\partial t} = -\beta(\hat{\phi})\frac{\partial \phi'}{\partial t} + \frac{1}{\hat{\phi}}\left[k'_d \frac{\partial^2 P'}{\partial z'^2} + \frac{\partial k'_d}{\partial z'}\left(\frac{\partial P'}{\partial z}\right)\right] + \frac{(\partial S'/\partial t')\gamma_S}{C'_v(\hat{\phi})}$$

where

$$\phi = \phi_0\left(1 + \frac{\Delta\phi}{\phi_0}\phi'\right), \qquad \hat{\phi} = \frac{\phi}{\phi_0}, \qquad t = \Delta t\ t', \qquad z = \Delta z\ z',$$
$$P = P_0 + P_0 P', \qquad S = \Delta S\ S', \qquad k_d = k_{d0}k'_d$$

and k_d, ϕ, S, C_v represent the permeability, porosity, entropy and specific heat capacity (averaged for grains and water), respectively. The scales Δz, Δt, ΔS, and $\Delta\phi$ are chosen to ensure that maximum variations of physical quantities, together with the dimensionless gravitational static pressure, are normalised to be $\mathcal{O}(1)$:

$$\Delta z = D_c\,, \qquad \Delta t = \frac{\phi_0 \mu P_0^2}{g^2 k_{d0} K_B \rho_0^2}\,,$$
$$\Delta S = \frac{C_{v0} P_0 \gamma_S}{\alpha K_B T_0}\,, \qquad \Delta\phi = \phi_0(1-\phi_0)\frac{P_0}{K_B}\,,$$

with $\mu, \rho, g, K_B, T, \alpha$ being the dynamic viscosity, density, gravitational acceleration, bulk modulus of water, temperature and coefficient of volumetric thermal expansion, respectively. In this case, peak inertial stresses are of the order $\rho_w \omega^2 a \Delta z = 8\times10^3 \mathrm{Nm}^{-2} = 0.08 P_0$ so $P' = 0.08$. For the Viper system the appropriate length scale is $0.04\,\mathrm{m}$ which is the full depth of the cake. In a deeper medium, the length scale for capillary rise would be $P_0/\rho_0 g \approx 0.4\,\mathrm{m}$ but this is outside the domain of the cake.

It is argued that fluidisation takes place if the timescale of the applied force (the loading) is shorter than the characteristic timescale on which the pressure grows, Δt (since pressure equalises with the boundary values on the timescale Δt). Combining the above equations leads to

$$\Delta t = \frac{(\Delta z)^2 \phi_0 \mu}{k_{d0} K_B}.$$

We assume typical values for water and silts of $\phi_0 = 0.5$ (comparable to $\theta_c = 0.45$), $\mu = 1.8 \times 10^{-3}$ kg m^{-1}s^{-1}, and $K_B = 2 \times 10^9$ N m^{-2}. From Section 2, $k_{d0} = K_c \mu / \rho_w g = 1.8 \times 10^{-14}$m^2. This leads to

$$\Delta t = 0.04\,\mathrm{s}.$$

With the Viper operating at 50 Hz, the loading time is $\Delta t_{\mathrm{load}} \approx 0.02\,\mathrm{s} = 0.5\Delta t$. This supports the idea that the Viper causes a liquefaction of the cake. This model does not include the vacuum suction.

As a side-note, we argue that small scale lab systems (on the scale of the vacuum belt under consideration) behave differently to geotechnical scales relevant for earthquakes. In fluidisation, flow/drainage should be unimportant in releasing stress if

$$\frac{\Delta P}{\Delta t_{\mathrm{load}}} \ll \frac{P_0}{\Delta t}.$$

In this case, the inequality is satisfied by a factor of 6.

4.3 Deborah number—solid versus liquid behaviour

As an alternative approach, we consider the Deborah number De, which quantifies the extent to which a material under an applied stress behaves like a solid or a liquid. Generally speaking, for $\mathrm{De} \ll 1$ the material behaves like a fluid, while for $\mathrm{De} \gg 1$ the material behaves more like a solid:. $\mathrm{De} \to \infty$ for a Hookean elastic solid; whereas $\mathrm{De} = 0$ for a Newtonian viscous fluid. The Deborah number is defined by

$$\mathrm{De} := \frac{t_d}{t_0}, \tag{15}$$

where t_0 is the timescale of the deformation and t_d is the characteristic timescale for relaxation of the stress.

Following Goren et al. (2011), we take the relaxation time as the timescale for equalisation of the pore pressure ("pore pressure diffusion"). If the pore

pressure is able to equalise with the boundaries (atmospheric value) between driving cycles, then the Viper cannot repeatedly build the pressure to reach the liquefaction threshold. Goren et al. (2011) take for the pore pressure diffusion timescale

$$t_d = \frac{l d}{D_w}, \qquad \text{where} \quad D_w = \frac{k}{\beta \mu \phi},$$

where d is the grain diameter, k is the permeability, ϕ is the porosity, μ is the dynamic viscosity of the fluid, β is the adiabatic fluid compressibility, and the length scale $l = \min(\zeta, D_w/c_0)$, with ζ the maximum distance to the boundary and c_0 a characteristic velocity for the perturbation. Goren et al. (2011) consider the effect of thin boundary layers of higher permeability, which are ignored for well-drained systems—we assume here a uniform permeability since the water is free to drain out of the top surface of the cake.

With speed of sound c_s, we take

$$\phi = 0.5, \qquad \mu = 1.8 \times 10^{-3}\,\mathrm{kg\,m^{-1}s^{-1}},$$
$$k = 1.8 \times 10^{-14}\,\mathrm{m^2}, \qquad \beta = \frac{1}{\rho c_s^2} \approx 10^{-9}\,\mathrm{Pa^{-1}},$$
$$d = 100\,\mu\mathrm{m} = 10^{-4}\,\mathrm{m}.$$

Over the compressive part of the Viper oscillation, the mean velocity is $-\frac{2}{\pi}\omega a = -4 a \nu = -0.4\,\mathrm{ms^{-1}}$. We find $\ell = \zeta = 0.04\,\mathrm{m}$, which is less than the diffusive length. Substituting all of these values into (15) we obtain $\mathrm{De} = 5 \times 10^{-3}$. This suggests that the Viper action causes the cake to 'flow', disrupting the established 'fingers' of air flow. The higher the frequency of the Viper, the shorter the timescale and the smaller the Deborah number. Even for the lowest mentioned operating frequency of 15 Hz the Deborah number is still well below one.

4.4 Macroscopic Darcy Picture During Liquefaction

Could partial liquefaction over such a short time have such an effect on water extraction? At the form line, the cake is saturated with negligible overlying water. During subsequent liquefaction the total volume cannot increase. Therefore the redistributed solid particles remain close together and the subsequent re-compaction time could be quite short. Assume that the cake takes at least as long to consolidate as it does to liquefy. Consider a time span of liquefaction to be $\Delta t = 0.4\,\mathrm{s}$. The equivalent depth ℓ of water removed by the Viper at 50 Hz is 3.2 mm. Assume that during liquefaction there remains a sediment of depth $D < D_c$. Given the effective hydraulic conductivity $K_s = \mathcal{K}(D)$, Darcy's law (2) then determines the approximate thickness D of the unbroken sediment pile beneath the liquefied layer:

$$-\mathcal{K}(D)\frac{c_1}{D} = \frac{\ell}{\Delta t}\,.$$

Numerically solving this for D, we obtain $D = 1.0\,\mathrm{cm}$. Above that layer of intact sediment there is a liquefied mixture layer around 2.6 cm thick. That depth of partial liquefaction would be proportional to the number of cycles of vibration. If the frequency is reduced from 50 Hz to 15 Hz, then the sediment pile should be reduced by 8 mm rather than 26 mm. The relation (7) for conductivity of compacted sediment would then predict a very low amount of additional water removed. However, the assumption of a constant conductivity during a nonlinear diffusion process leads to errors. The observations indicate an extra outflow of 1.6 mm at 15 Hz. The question arises whether during shaking, the remaining sediment bed has some dynamical response that reduces hydraulic conductivity. Contrary evidence is that the Viper gives no discernible improvement to water extraction in the nearby slurry zone with underlying sediment. The liquefaction theory, combined with Darcy flow, does at least incorporate some frequency dependence. The criteria for liquefaction include the number of cycles and the peak stress, both of which increase with frequency.

5 Representation of Solid Fraction on Whole Belt

The content of water as it travels along the vacuum belt were considered in three parts, each of which are subjected to different physical mechanisms:

- the region with overlying slurry upstream of the form line;
- the saturated cake under the roller and Viper;
- the unsaturated cake further downstream.

Since each of these regions requires a different dynamical model, it is convenient to construct a simple smooth function that describes the x-dependent solid mass fraction along the whole belt. From a high input value of $1 - f_s \in [0.75, 0.87]$, the gravimetric water content rapidly diminishes. That rapid decrease is approximated by an exponential function. A simple composite model approximates the trend of the data before the form line, while there is an observed flatness once the cake has formed. Upstream the solids fraction is dominated by the component

$$f_s(\text{upstream}) = C - Ae^{-Bx}, \tag{16}$$

Near the Viper location $x = x_V$, the upstream component connects to a flat downstream component by the addition of the simple sigmoid component function

$$f_s(\text{Viper}) = \frac{E}{1 + \exp\left([x_V - x]F\right)}. \tag{17}$$

By adding the two components the solids fraction along the whole belt is approximated as

$$f_s = C - Ae^{-Bx} + \frac{E}{1 + \exp\left([x_V - x]F\right)}.$$

An example of optimised values to fit this equation in the case of a coal slurry on a vacuum belt moving at $8\,\mathrm{m\,s^{-1}}$ and the Viper module operating at $50\,\mathrm{Hz}$

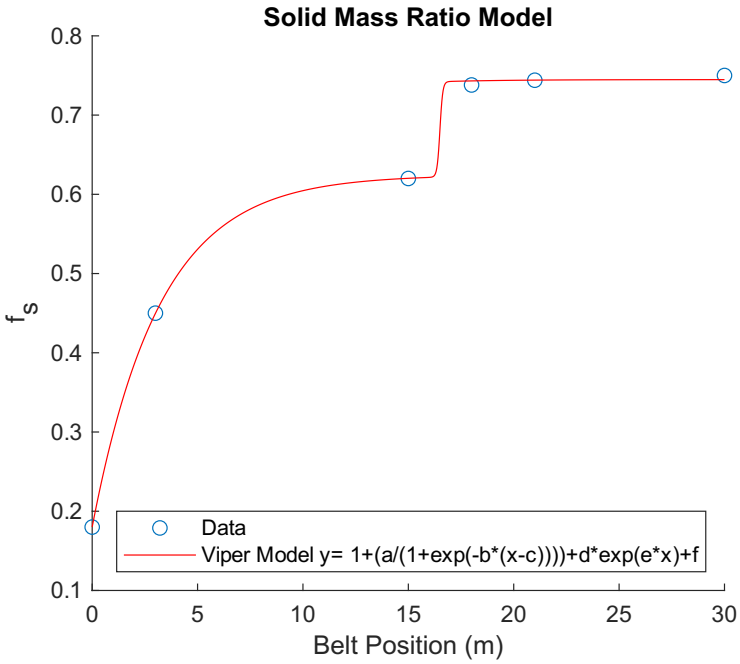

Figure 5: Fitting solid mass ratio versus x over the entire belt length using exponential functions.

are

$$A = 0.4443\,, \qquad B = 0.3111\,, \qquad C = 0.6244\,,$$
$$E = 0.1204\,, \qquad F = 15\,, \qquad x_{\text{Viper}} = 16.50\,.$$

These values are for respective constants in (16) and (17). These variables correspond to the fit of the data shown in Figure 5.

The model can accurately represent current data in a variety of situations such as varied frequency and belt speed. However, compared to the Darcy flow model (4), the values of f_s between Stations 1 and 2 are higher, and flatter as Station 2 is approached.

6 Improving Efficiency by Belt Speed and Multiple Vipers

The data show that adding a second Viper does improve water extraction but only by a relatively small amount. At a short distance past the first Viper, in the region of re-consolidation, the matrix structure is more rigid, allowing little more compression. There is then no more liquid lying above the cake. Further exit of water from the cake can happen only by air displacing the liquid from the larger pores. The medium is then unsaturated, with the remaining water held in progressively smaller pores whose conductivity is lower, in proportion to pore radius squared. The conductivity decreases further along the belt and exiting water flux decreases. This is exacerbated by energy being wasted as work is done against friction as air is driven by the pressure gradient through larger pores. The data show that little more water is extracted more than a few metres beyond the first Viper. A second Viper achieves little more because it must be placed over a compacted drier cake with higher hydraulic resistance. If it is to be used, then both Vipers should be placed close together in the early part of the formed cake. However, the theory of liquefaction followed by consolidation would have the second Viper working on a more cohesive cake that would be held together more strongly by surface tension even when it is saturated. Shaking would then remove fewer solid grains and a second liquefaction would be more superficial.

Increasing belt speed does increase throughput. However, the data show that not so much water is removed when the speed u_0 is increased from $14\,\mathrm{cm\,s^{-1}}$ to $20\,\mathrm{cm\,s^{-1}}$. With one Viper operating, the final solid mass fraction decreases from 75% to 72% and with two Vipers, the decrease is from 75.6% to 72.6%. The decrease in performance is partly due to the water flow through the cake taking place over a shorter time. However, when a Viper is operating, we have already seen that relatively little water is extracted over the last $8\,\mathrm{m}$ of the belt. This suggests that the reduction is due to a shorter interaction time as the cake passes under the roller. As f_s reduces from 0.75 to 0.72,

the depth of water removed from the saturated cake decreases from 6.8 mm to 5.6 mm. As the speed is increased from 14 cm s^{-1} to 20 cm s^{-1}, interaction time with the roller decreases by 30% and the remaining depth of water in the cake increases by 1.2 mm which is 48% of the water removed by the Viper at 50 Hz up to Station 3 when the belt speed is at the lower value.

7 Conclusion

De-watering through a vacuum filter belt involves three distinct stages. In the first stage, a liquid slurry lies above a growing sediment layer. We have shown that the observed rate of extraction is in accord with Darcy's law after assuming reasonable values for the hydraulic conductivity of the sediment and filter mat. However, we can obtain exact agreement with the data only when the hydraulic conductivity decreases with time. This reflects the entry of fine particles into large pores. We have not yet accounted for the consequent decrease in porosity (and consequent decrease in saturated water content) that happens over a short time before fine particles fill the largest pores. Generally speaking there is not a large variation in porosity across soil types.

It has been found that the vibrating Viper is most effective in the narrow region of the second stage, just after the form line of the solid filter cake. Our calculations indicate that, due to its lower viscosity, air will form low-viscosity fingers that will fully penetrate from the surface to the bottom of the cake in a short time, thereby short-circuiting the effectiveness of the pressure gradient to drive water flow.

One role of the Viper is to break up the fingers, restoring useful water flow for a short time. Although our calculations, accounting for viscosity of the fluid mixture, suggest that a second Viper should optimally be placed at 1.4 times the distance from the form line compared to the first Viper. By that distance we anticipate that the filter cake will be drier and more rigid, and we expect that it will be more difficult for a second Viper to break up the air fingers.

A second role of the vibration is to effect temporary liquefaction of the mixture, thereby again improving downward water flow. This is not independent of finger break-up which involves the mixing of solids and fluids. Although there is no universally accepted theory of observed liquefaction of vibrating soils, a currently published theory does account for near-complete liquefaction at the water content and maximum Viper vibration frequency.

Downstream reformation of fingers would further decrease water flow, even beyond the decrease predicted in Darcian one-dimensional unsaturated flow.

The third stage is far downstream where the formed filter cake is unsaturated and it contains a large amount of air. It is found experimentally that little additional water is extracted during that stage. This also is in accord with standard Darcian soil-water theory wherein hydraulic conductivity rapidly decreases as water content decreases. A full solution for the nonlinear boundary value problem of one-dimensional unsaturated flow through the formed cake, is achievable with current mathematical technology but that would require a lot of work. The one-dimensional model neglects viscous fingering. Therefore despite already predicting a minor level of water extraction through the formed cake, it would be an over-estimate. That amount of water extraction is barely significant for this industrial process.

Some errors in our modelling result from assuming quasi-one-dimensional flow which neglects horizontal flow of water. The solution of the full two-dimensional flow problem would be moderately challenging, especially since two free surfaces are involved. In the future that could be tackled by computational fluid dynamics software.

We identified some mechanisms that have not yet been verified by more detailed experiment. The problem could be better understood when the theory of liquefaction is more developed. Given the small length and time scales involved it should be possible to set up a small lab scale experiments, perhaps using a centrifuge to produce the required driving force.

References

Broadbridge, P. and P. J. Banks (1992). "Exact Nonlinear Solution for Constant-Rate Expression from Material of Finite Thickness". In: *J. Austral. Math. Soc. (B)* 33, pp. 30–50 (cit. on p. M34).

Chuoke, R.L., P. van Meurs, and C. van der Poel (Aug. 1959). "The Instability of Slow, Immiscible, Viscous Liquid-Liquid Displacements in Permeable Media". In: *Petroleum Transactions, AIME* 216, pp. 188–194 (cit. on pp. M34, M38, M39).

Goren, L. et al. (Dec. 2011). "The Mechanical Coupling of Fluid-Filled Granular Material Under Shear". In: *Pure and Applied Geophysics* 168.12, pp. 2289–2323. DOI: 10.1007/s00024-011-0320-4 (cit. on pp. M42, M44, M45).

Lakeland, D. L., A. Rechenmacher, and R. Ghanem (Feb. 2014). "Towards a complete model of soil liquefaction: the importance of fluid flow and grain motion". In: *Proceedings of the Royal Society of London Series A* 470.2165, p. 20130453. DOI: 10.1098/rspa.2013.0453 (cit. on p. M42).

Mahesar, Aftab et al. (2017). "Comparison of Klinkenberg-Corrected Gas and Liquid Permeability in Kirthar Fold Belt Tight Gas Sands". In: *Mehran University Research Journal of Engineering and Technology* 36.4, pp. 957–964. URL: https://hal.archives-ouvertes.fr/hal-01705503/document (cit. on p. M37).

Raats, P. A. C. and J. H. Knight (2018). "The Contributions of Lewis Fry Richardson to Drainage Theory, Soil Physics, and the Soil-Plant-Atmosphere Continuum". In: *Frontiers in Environmental Science* 13, pp. 1–15 (cit. on p. M32).

Saffman, Philip G. and Geoffrey Taylor (1958). "The penetration of a fluid into a porous medium or Hele-Shaw cell containing a more viscous liquid". In: *Proc. Roy. Soc. A* 245, pp. 312–329 (cit. on pp. M33, M34, M35, M38).

Sawicki, Andrzej and Jecek Mierczyński (Jan. 2006). "Developments in Modeling Liquefaction of Granular Soils, Caused by Cyclic Loads". In:

Applied Mechanics Reviews 59.2, p. 91. DOI: 10.1115/1.2130362 (cit. on p. M42).

Smith, R. E. et al. (2002). *Infiltration Theory for Hydrologic Applications*. Amer. Geophysical Union (cit. on pp. M25, M26).

White, I. and P. Broadbridge (1988). "Constant Rate Rainfall Infiltration: A Versatile Non-linear Model. 2. Applications of Solutions". In: *Water Resources Research* 24, pp. 155–162 (cit. on pp. M29, M32, M34).

Author addresses

1. **P. Broadbridge**, School of Computing, Engineering and Mathematical Sciences, La Trobe University, Victoria, Australia
orcid:0000-0003-1784-5344
2. **S. Caldwell**, Jord International, NSW, Australia
3. **T. Marsh**, Dept. of Physics, University of Newcastle, Australia
orcid:0000-0001-8162-5595
4. **M. McGuinness**, School of Mathematics & Statistics, Victoria University of Wellington New Zealand
orcid:0000-0003-1860-6177
5. **O. Orozovic**, School of Engineering, University of Newcastle, Australia
orcid:0000-0001-5155-9822
6. **D. I. Pontin**, School of Information & Physical Sciences, University of Newcastle, Australia
orcid:0000-0002-1089-9270
7. **A. Raboonik**, School of Information & Physical Sciences., University of Newcastle, Australia
orcid:0000-0002-6408-1829

8. **K. Stevens**, School of Information & Physical Sciences, University of Newcastle, Australia
mailto:kyle.stevens@uon.edu.au
orcid:0000-0001-8226-9510